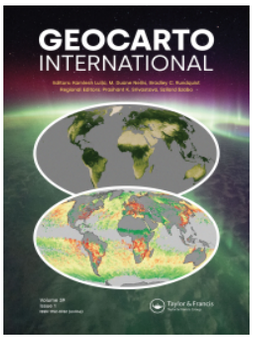

Geocarto International

ISSN: (Print) (Online) Journal homepage: www.tandfonline.com/journals/tgei20

Results of high-resolution technologies applied in the acquisition of seafloor information in the Colombian Caribbean Sea

Karem Oviedo-Prada, Juan J. Muñoz-Perez, Germán Escobar-Olaya, Ana Maria Osorio-Granada, Stephan Howden, Cristina Torrecillas-Lozano, Jeanette Romero-Cozar, Antonio Contreras-de-Villar, Hermann Leon-Rincon & Bismarck Jigena-Antelo

To cite this article: Karem Oviedo-Prada, Juan J. Muñoz-Perez, Germán Escobar-Olaya, Ana Maria Osorio-Granada, Stephan Howden, Cristina Torrecillas-Lozano, Jeanette Romero-Cozar, Antonio Contreras-de-Villar, Hermann Leon-Rincon & Bismarck Jigena-Antelo (2024) Results of high-resolution technologies applied in the acquisition of seafloor information in the Colombian Caribbean Sea, Geocarto International, 39:1, 2321365, DOI: 10.1080/10106049.2024.2321365

To link to this article: https://doi.org/10.1080/10106049.2024.2321365

Published online: 11 Mar 2024.

GEOCARTO INTERNATIONAL
2024, VOL. 39, NO. 1, 2321365
https://doi.org/10.1080/10106049.2024.2321365

Taylor & Francis
Taylor & Francis Group

Results of high-resolution technologies applied in the acquisition of seafloor information in the Colombian Caribbean Sea

Karem Oviedo-Prada[a,b], Juan J. Muñoz-Perez[a], Germán Escobar-Olaya[b], Ana Maria Osorio-Granada[a,b], Stephan Howden[c], Cristina Torrecillas-Lozano[d,e], Jeanette Romero-Cozar[a], Antonio Contreras-de-Villar[a], Hermann Leon-Rincon[b] and Bismarck Jigena-Antelo[a,c]

[a]Universidad de Cádiz, Campus de Puerto Real, CASEM, Puerto Real, Spain; [b]Oceanographic and Hydrographic Research Centre of the Caribbean, Cartagena de Indias, Colombia; [c]Hydrography Science Research Center, University of Southern Mississippi, Long Beach, MS, USA; [d]Departamento de Ingeniería Gráfica, Universidad de Sevilla, Sevilla, Spain; [e]Kongsberg Maritime Training Center, Boca del Río, Veracruz, Mexico

ABSTRACT

We expound on a hydrographic and geophysical survey in the south of the Archipelago of San Andres, Providencia, and Santa Catalina (ASAPSC) in the Colombian Caribbean Sea. In 2017 and 2018, high-resolution data were acquired from the Caribbean Center for Oceanographic and Hydrographic Research (CIOH). The hydrographic data were processed and filtered per International Hydrographic Organization (IHO) standards and the geomagnetic data were processed, corrected, and filtered to improve the interpretation. We could then characterise the submarine relief, analyse the geomagnetic anomalies in the area, and identify different relief forms of volcanic origin. Regarding geomagnetic work, a spectral analysis of the anomalies revealed highly magnetic bodies in deep water and residual magnetic anomalies strongly related to the seabed morphology. Magnetic highs associated with the basement highs and volcanic cones were detected. Complementary spectral analysis showed that the shallowest magnetic sources were in the first 500 m, whereas the deepest magnetic sources were between the depths of 4 and 5 km. The geomagnetic data were also validated using Euler deconvolution analysis, which confirmed these magnetic anomalies. Thus, a direct relationship between the magnetic anomalies and bathymetry of the seafloor was confirmed, reinforcing the theory of the volcanic origin of these islands.

ARTICLE HISTORY
Received 31 July 2023
Accepted 15 February 2024

KEYWORDS
Colombian Caribbean Sea; ASPSC; bathymetry; magnetic anomalies; marine geo-physics

CONTACT Bismarck Jigena-Antelo bismarck.jigena@gm.uca.es

1. Introduction

Magnetic methods for geological applications were developed in 1630 in Sweden, with a focus on iron ore prospecting (Hanna 1990). In the oil industry, these have been used as reconnaissance methods in regional surveys since the beginning of the last century (López-Loera et al. 2013). Marine magnetic anomalies are used to investigate the extent of the seafloor and the transition between continental crust and oceanic crust at passive margins and zones with high iron content (Granot and Dyment 2019). Potential theory methods (Telford et al. 1990; Blakely et al. 2002) have enabled magnetometry to become a source of information for studying fault zones and their possible reactivations (Blakely et al. 2002). It has also been used to evaluate the magnetic properties of volcanoes (Finn and Williams 1987; Berrocoso Domínguez et al. 2018), establish the existence of volcanic magnetic belts, and study their relationship with geodesy and topography (Flanagan and Williams 1982; Honkura et al. 1991; Bernabéu et al. 2001; Jigena et al. 2016). Magnetic methods have also been used to locate intrusive bodies in subsurfaces with no surface manifestations (Finn and Williams 1987; Oviedo et al. 2020).

The first geomagnetic data for the study area were obtained in the early 1970s. Two research cruises led by the National Oceanic and Atmospheric Administration were conducted. Several authors have described the western Colombian Caribbean Sea(e.g. Geister 1992; Geister and Diaz 2007) as a volcanic province with coral formations (Figure 1). Several theories and magnetic studies of the Caribbean Sea have been conducted with different hypotheses, such as Driscoll and Diebol (1998), denoting the presence of a fracture in a plate as evidence of two plates instead of one. (Catalán and Martos 2022) suggested the presence of local anomalous bodies that could be correlated with volcanic structures, which generated concerns about more specific areas.

From multibeam bathymetry data, a series of submarine geoforms have been identified south of San Andres Island, such as depressions of tectonic origin (the San Andres,

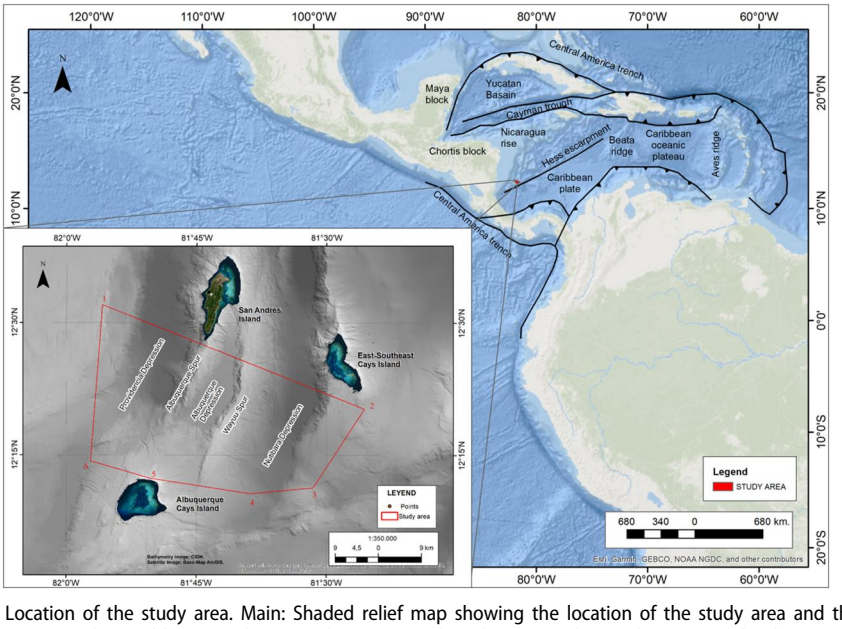

Figure 1. Location of the study area. Main: Shaded relief map showing the location of the study area and the major tectonic features in the Caribbean. In the inset shows zoomed study area in the northwestern Colombian corresponding to the red polygon. Grey shows the CIOH high-resolution bathymetry. The blue background shows the ArcGIS Ocean base map.

Albuquerque, and Nutibara Depressions), volcanic spurs (Albuquerque and Wayuu Spurs), and a series of fault systems, mostly in the NNE-SSW direction (Idárraga-García and León 2019). Based on such bathymetry, there is an imminent need to increase the number of geological and geophysical studies in this area to identify magnetic anomalies that may be associated with volcanic bodies and submerged reefs (Oviedo et al. 2020).

The bathymetry influences the magnetic response because it is highly dependent on the distance from the sensor to the seabed. Therefore, if there is shallow bathymetry, the magnetic response will be stronger than that of the same source in deeper bathymetry. In addition, we must consider that the magnetic response depends on the presence of magnetic materials in the rock; however, as mentioned previously, it also depends mainly on the distance to the source. This study was based on the assumption that a clear correlation exists between the elevations of the measurement point magnetic field for a relatively homogeneous magnetic medium. In the case of direct magnetisation, the field maxima correspond to the crests of the 'magnetic' relief, while the minima correspond to the valleys (Eppelbaum 2019).

The main contribution of this study was to test the implementation of the marine geomagnetic method developed by the National Hydrographic Service of Colombia (Oviedo et al. 2020; CIOH 2024). This project was motivated by the lack of information on the magnetic signatures of the complex of islands, atolls, and reefs, and the need to complement the physiographic descriptions made by the authors mentioned above. Finally, the objective of this study was to demonstrate the usefulness of high-resolution surveys for detecting magnetic anomalies and improving seafloor relief information. For this purpose, the methodology and results of its application to a zone in the Colombian Caribbean are presented.

2. Geological background

2.1. Study area

This study tests the implementation of the marine geomagnetic method developed by the Colombian National Hydrographic Service (Quintero et al. 2014) and is motivated by the lack of information on the magnetic signatures of the island complex, which can complement the physiographic descriptions made by other authors (Rey et al. 2021; Zou et al. 2021). In addition, although the study area is small (1050 km^2), it has great geological, geomorphological, and oceanographic diversity (Payo et al. 2018; Rey et al. 2021; Jigena-Antelo et al. 2023).

The ASAPSC is located in the western Colombian Caribbean Sea. It extends from 12° N latitude and from the border with Panama in the southwest (SW) at 79° W longitude to the Guajira Peninsula in the northeast (NE) at 81° W. The study area is delimited by the island of San Andres and a group of smaller cays represented by atolls and coral reefs (Geister 1992; UN 1982) (Table 1).

Table 1. The coordinates that delimit the area.

Vertex	Latitude (N)	Longitude (W)
1	12°31′50.91"N	81°55′44.07"W
2	12°20′15.26"N	81°25′37.20"W
3	12-11′23.59"N	81°31′28.24"W
4	12°10′35.44"N	81°38′51.98"W
5	12°12′23.75"N	81°50′12.05"W
6	12°14′16.47"N	81°57′8.33"W

Freely accessible data only offer a solid foundation in a broad sense due to their resolution limitations. The GMRT bathymetric model and the EMAG2 magnetic model reflect distinct curves and have no direct relationship. EMAG2v3 has been used which does not use any prior age information. It follows that hydrographic and geophysical surveys yield relatively little information due to their lack of resolution and detail. In fact, if a more thorough study is required, high-resolution data must be obtained using suitable survey techniques that enable the processing and creation of investigative-style final products.

2.2. Geological and tectonic context

Geologically, ASPSC is located in the western part of the Caribbean Plate. This plate is located in the middle of the Cocos, Panama, North Andes, South America, and North America plates. The evolution of the Caribbean Plate throughout the Cenozoic was controlled by sediment accumulation, structural deformation of the pre-existing crust, and volcanism.

The study area is part of a geological province known as the Lower Promontory of Nicaragua (LNR) (UN 1982), which is a crustal block bounded to the northwest by the Pedro Escarpment and to the southeast by the Hess Escarpment, a zone of distensive character since the Middle Miocene (Holcombe et al. 1990; Mauffret and Leroy 1997). Recently (Case et al. 1990), based on gravimetry, magnetic modelling, and integration with seismic data, it has been concluded that the LNR is composed of oceanic crust (Carvajal Arenas 2017; Osorio-Granada et al. 2022).

It has been proposed that the tectonic evolution of the region started from two eroded volcanic cones whose geological history is closely related to the evolution of the Nicaraguan High and part of the Caribbean Plate (Case et al. 1990; Pindell et al. 2006). It was concluded that the atolls, islands, and coral banks may have originated from volcanic activity during the Early Cenozoic (Geister and Diaz 2007). Within the study area, the main structures are as follows:

San Andres Island: The age is estimated to be Palaeogene, which is compatible with the geological history of the western Caribbean crust. The simultaneous subsidence and carbonate production in the Miocene shallow sea resulted in the formation of a thick atoll-type limestone bank at the top of the volcanic structure (Geister 1992).

Albuquerque Cays Island: This atoll is the only one with a circular outline. According to palaeomagnetic data from a sample of a fragment of basaltic lava obtained from its northwestern slope at a depth of approximately 700 m, the atoll has a volcanic basement (Milliman 1969).

East-Southeast Cays Island: The southern half of the atoll has a SE-NW orientation, while the northern half shows a clear NNE-SSW direction. This could indicate an important site for the triple intersection of the two fault zones with different strike slips that underlie the presumed volcanic cone that appears to form the basement of the atoll (Geister and Diaz 2007).

3. Data and methods

3.1. Bathymetric survey

Bathymetric data were acquired between August and September 2017. On board the Oceanographic Research Vessel of the Colombian Navy 'ARC Providencia', a Kongsberg

model EM302 multibeam system with an operating frequency of 30 kHz was used (Kongsberg 2023).

The bathymetric survey in the area was composed of approximately 38 lines perpendicular to the general direction of NNE geology with an average length of 70 km. For the shallow waters adjacent to the emerged area of the islands, increasing the density of the lines was necessary to cover the whole zone while maintaining the overlapping (Oviedo et al. 2020; CIOH 2024). As a result, a bathymetric chart at the study area with a spatial resolution of 35 m per pixel was obtained.

The software used for hydrographic data collection is the Sea Information System (SIS) configured with an opening angle of 70°, performing a 30% overlap seeking to ensure 100% bottom coverage, according to IHO (International Hydrographic Organization) standards (IHO 2020). Additionally, differential positioning with the Seapath system was used, which guarantees centimetre accuracy in the bathymetric survey. For the horizontal and vertical referencing of hydrographic data, a previously proposed methodology (Jigena et al. 2015, 2016; Nwankwo et al. 2020) has been used.

3.2. Geomagnetic survey

Geomagnetic data were acquired aboard ARC Roncador between 20 June and 1 July 2018. A G-882 magnetometer with a sampling rate of 20 Hz was used (IHO 2020). It was towed at 150 m from the vessel at an average speed of seven knots. The positioning system used for the sensor was Trimble R7 with real-time correction in the WGS84 reference system (Berrocoso Domínguez et al. 2008; Jigena et al. 2016; Oviedo et al. 2020; Nwankwo et al. 2020). The implemented geometric arrangement for magnetometry considered a line spacing of 12 km, and a spatial resolution of 500 m per pixel was obtained.

Data collection was performed using MagLog software. Total Magnetic Field was calculated in nT, with a typical sensitivity of 0.02 nT at 0.1 s sample intervals, operating over an operating range of 20,000 nT to 100,000 nT (Geometrics Inc 2018).

The geophysical survey comprised four lines perpendicular to the general direction of the geological structures NNE (lines 1, 2, 3, and 4) with a maximum length of 70.67 km, and four lines parallel to the formations (lines 5, 6, 7, and 8) with a maximum length of 31 km (see Figure 10 in Oviedo et al. 2020).

3.3. Processing

The geomagnetic data were processed using the Oasis Montaj software, version 8.5.5, Geosoft (Seequent 2022). The data were corrected for diurnal variation, delay correction, orientation correction in degrees, and the International Geomagnetic Reference Field.

For diurnal variation correction, magnetometric readings were recorded simultaneously with the marine acquisition, using the RBS G-862 base magnetometer installed at Cartagena de Indias city (Colombia) at the following coordinates: latitude north 10°23'24.62, and longitude west 75°31'54.97. During this procedure, the data acquired from the RBS G-862 base magnetometer were subtracted from those obtained using the G-882 mobile magnetometer (Grandis and Dahrin 2017; Seequent 2022). In the correction process, a longitudinal difference of 6° was considered; unfortunately, owing to logistical aspects, it was impossible to instal it closer to the study area so that it would be within the ideal 1° distance. Additionally, it is important to highlight that diurnal variation correction data were applied because it was verified that there were no solar storms or major variations that could affect the results of the correction process.

For delay correction, the first five data points of each line were discriminated, seeking to eliminate the data that were taken while the sensor was not yet al.igned on the planned survey line, to reduce the uncertainty of the data due to turning manoeuvres of the vessel at the time of acquisition (Grandis and Dahrin 2017).

For the correction of orientation in degrees, the changes in sensor orientation during acquisition were considered, and the uncertainties generated in these directions were calculated. This has been corrected according to the methodology presented in the user manual (DIMAR et al. 2015; Oviedo et al. 2020).

For the IGRF correction, the model values (Alken et al. 2021) were subtracted for each survey point, considering the inclination and magnetic declination. A value was assigned depending on the latitudinal position in the study area and subtracted from the database.

Finally, with the corrections, a total field anomaly map was generated, which became the basis for the elaboration of the visualisation filters. All the maps were generated using the minimum-curvature interpolation method. The following filters were used.

A reduction to the pole was applied to the total field anomaly grid to eliminate the effect of the tilt of the magnetic anomalies by transforming the anomaly as if the source had been read at the magnetic pole with a 90° tilt (Bajgain 2011). The pole reduction can be calculated in the frequency domain using the following operator: (MacLeod et al. 1993):

$$\boldsymbol{L}(\boldsymbol{\theta}) = \frac{1}{\left[sin(\boldsymbol{I}) + icos(\boldsymbol{I})cos(\boldsymbol{D} - \boldsymbol{\theta})\right]^2} \tag{1}$$

Where:

θ is the wavenumber direction

I is the magnetic inclination

D is the magnetic declination.

nT was used in the SI for the magnetic field variations measured in the geophysical surveys.

The first vertical derivative was applied to the resulting grid of the total anomaly field to highlight linear features, accentuating pronounced bathymetric features. This procedure is related to deeper sources (Jacobs 1994), mapping of deep basement structures, and mineral exploitation targets (Seequent 2022).

An analytical signal filter is applied to enhance the potential field anomaly. It is used to define the boundaries of geologically anomalous density or magnetisation distributions (Alatorre-Zamora et al. 2012). The filter is defined as the square root of the sum of the derived squares in the x, y, and z directions: This is useful for locating the edges of the magnetic source bodies (Narvaez Medina 2012). The application of the analytic signal shows the shape of the bodies and their possible locations, but not the direction of magnetisation. The following formula describes this mathematically (Galvan 2016):

$$\left|\boldsymbol{B}(\boldsymbol{x},\boldsymbol{y},\boldsymbol{z})\right| = \sqrt{\left(\frac{\partial \boldsymbol{B}}{\partial \boldsymbol{x}}\right)^2 + \left(\frac{\partial \boldsymbol{B}}{\partial \boldsymbol{y}}\right)^2 + \left(\frac{\partial \boldsymbol{B}}{\partial \boldsymbol{z}}\right)^2} \tag{2}$$

To filter, visualise, and analyse possible features of the geomorphology, or to identify sources of seabed anomalies, we used the residual component with the following analyses:

Spectral analysis and Euler deconvolution inversion (DoE) were used and are defined as follows:

For the residual component, separation of the regional and residual anomalies was sought. This method uses the logarithm as a function of the wave number k, which is called interactive filtering

in the software. The deep characteristics that generate variations in the field observed on the surface on a regional basis and that present a long wavelength with smooth and gradual horizontal gradients are analysed. (DIMAR et al. 2015).

Normally, regional anomalies are attributed to deep (crustal) causes of large wavelengths, which generally influence the entire surveyed area in approximately the same manner. On the other hand, residual anomalies have small wavelengths and occur close to the measurement point.

The Gaussian filter with a cutoff frequency k_0 is defined as

$$L(k) = 1 - e^{-k^2/{}_2 k_0^2} \tag{3}$$

Where:

$$k = \sqrt{K_x^2 + k_y^2} \tag{4}$$

The absolute value of the wave number.

This filter then passes through small wavelengths corresponding to residual-type signals (Galvan 2016).

For spectral analysis, the logarithmic spectrum of these data can be interpreted as the depth of a 'set' of sources that is easily determined by measuring the slope of the energy (power) spectrum and dividing by 4π (Whitehead and Musselman 2007).

Euler deconvolution is based on the concept that magnetic fields are homogeneous functions of the source coordinates, and therefore satisfy the Euler equation. This equation can parametrically solve the source locations (Narvaez Medina 2012) by employing structural indices to evaluate the appropriate solution results (Geometrics Inc 2020).

A complementary method to the previous one is that proposed by Parker and Huestis (1974), which relates the reversal of magnetic anomalies to the presence and changes in the topography of the seabed. This method, which will be used in future research, can filter the effects of bathing on magnetic signatures.

4. Results

4.1. Geoforms obtained from the bathymetric survey

Using the CARIS HIPS and SIPS hydrographic software, (Teledyne 2021), the information was processed and exported to the GeoTIFF format (Figure 2) with a 35 m spatial resolution. The GeoTIFF data were exported to ArcGIS software, in which a digital elevation model was generated outlining contours every 100 m to scan bathymetric profiles (Figure 3).

From the bathymetric survey, surfaces ranging from 400 m to 1800 m deep were obtained. Profiles that helped in the characterisation of the submarine relief were drawn (Figure 3).

From west to east, the geomorphology of the study area is represented by:

Providencia Depression: To the west of San Andres Island, it has a general NNE-SSW trend and reaches an amplitude of approximately 10 km. A range of depths is identified between −1900 m in the deepest zone and −850 m in the shallowest part located towards the southwestern part of San Andres Island (Figure 3).

Albuquerque Spur: Connects the seamount of Albuquerque Cays Island with the seamount that makes up San Andres Island. The spur has an elongated morphology. Its general trend is NNE-SSW, reaching a length of approximately 18 km and rising approximately 1000 m from the seafloor. Depths range from −300 m to −1100 m in the deepest zone (Figure 3).

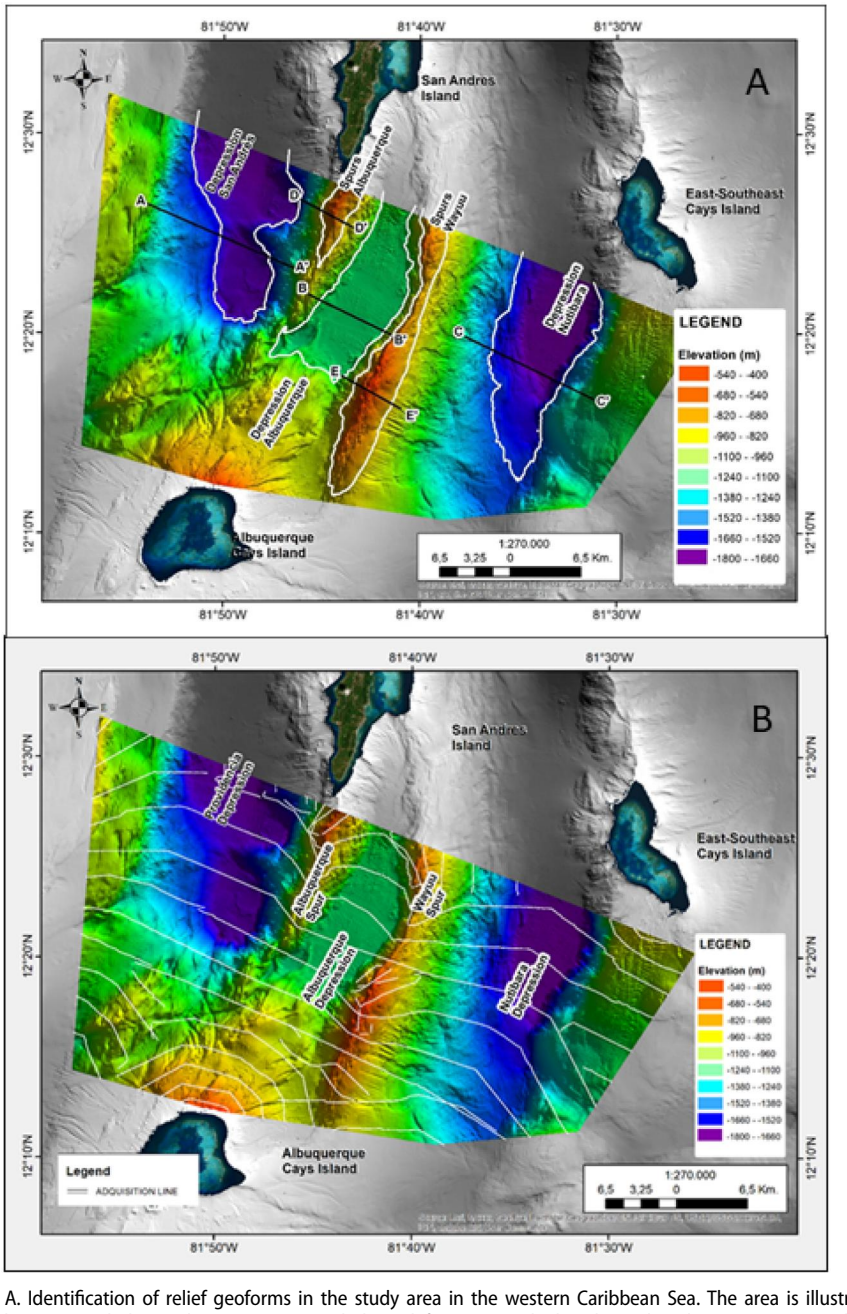

Figure 2. A. Identification of relief geoforms in the study area in the western Caribbean Sea. The area is illustrated by colour bathymetry and shows the main geomorphological features marked with a white line representing the maximum depth for each geoform (1800 m for the San Andres Depression, 600 m for the Albuquerque and Wayuu Spurs, 1100 m for the Albuquerque Depression and 1700 m for the Nutibara Depression). Bathymetric profiles (AA', …, EE') are also represented. B. Trackline Survey Plot of the multibeam data collected by ARC Providencia.

Albuquerque Depression: Located between the Albuquerque and Wayuu Spurs, this is a small depression with an average depth of −1180 m. It extends from the northeastern sector of the Albuquerque seamount to the southeastern tip of San Andres Island (Figure 2). It is 6 km wide, varying from 3.46 km at its narrowest part to 7.24 km at its widest point. The profile shown in Figure 3 indicates a depth variation ranging from −500 m to −1100 m.

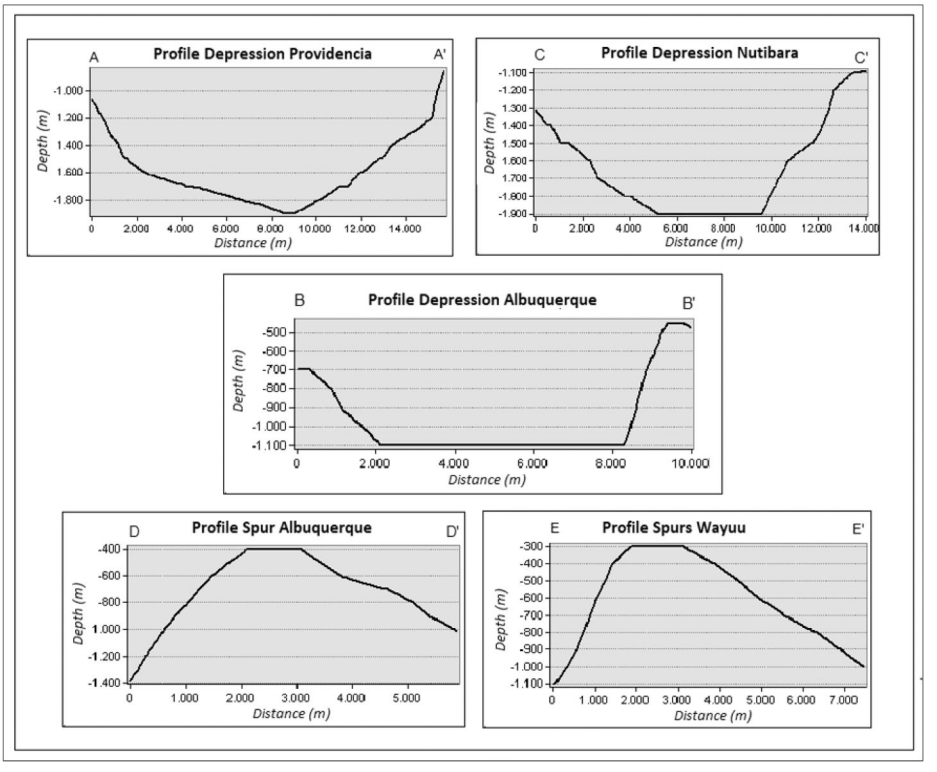

Figure 3. Bathymetric profiles showing the main geoforms of the study area (A) Providencia Depression, (B) Albuquerque Depression, (C) Nutibara Depression, (D) Albuquerque Spur, (E) Wayuu Spur. See Figure 2 for the location of the profiles.

The Wayuu Spur: Located southeast of San Andres Island. It connects the seamount of Albuquerque Cays Island with the seamount that configures San Andres Island. It is 37.18 km long and averages 2.90 km in width. Depths range from −300 m in the shallowest part to −1400 m in the deepest zone (Figure 3).

The Nutibara Depression is located southwest of East-Southeast Cays Island. It extends for approximately 55 km from the northeastern sector of Albuquerque to the northeastern sector of the island of San Andres, reaching a maximum depth of −2180 m and a maximum width of approximately 7 km. It has a maximum depth of approximately −1900 m and an average width of 8.3 km. The depth of the shallowest zone was approximately −1100 m (Figure 3).

4.2. Magnetic anomalies

In the total magnetic field map of the study area, magnetic intensities ranging from −292 nT to 205 nT are observed. The information grid shows a magenta magnetic maximum located at the limits of the Wayuu Spur and the Nutibara Depression (Figure 4). In contrast, the area near Albuquerque Cays Island is represented by the magnetic minimum, shown in blue.

The pole reduction reaffirms the maximum value of the positive anomalies with a northeast alignment between the Wayuu Spur and Nutibara Depression; this value is expressed in a value of 343.30 nT (Figure 4). The blue-coloured magnetic lows are represented by values up to −361.61 nT located towards Albuquerque Cays Island. It was observed that the magnetic lows tended to increase with decreasing depth, similar to the geomorphology of Albuquerque Cays Island.

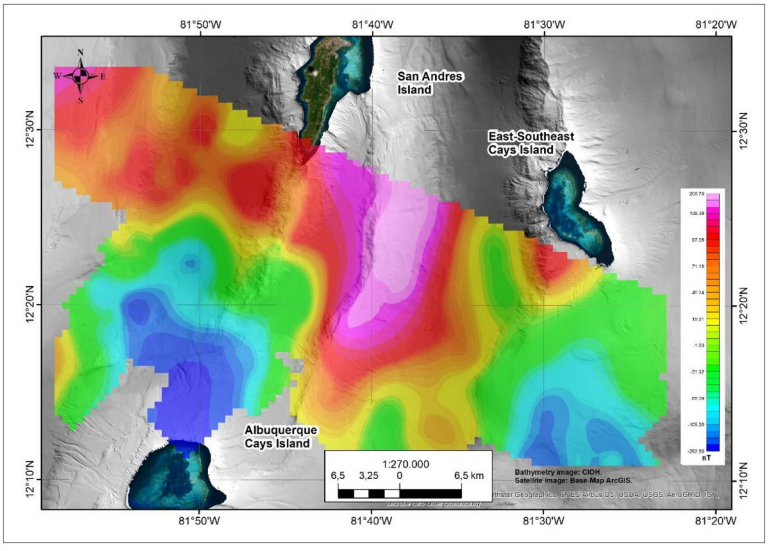

Figure 4. Magnetic pole reduction map of the study area. Magnetic surface reflecting the process of positioning correction for latitudinal effects. Grey background is the CIOH high-resolution bathymetry.

The analytic signal filter preserves the magnetic highs in the northeast lineament over the Nutibara Depression (Figure 5) but is more pronounced towards the southern part of the Nutibara Depression. New magnetic highs are visible towards the western part of the grid in a punctual and centralised manner. The magnetic surface values range from 0.0019 to 0.1007 nT/m (Figure 5).

The filter of the first vertical derivative of the inclination of the residual magnetic field shows a line of four magnetic maxima in yellow over the Wayuu Spur in the northeast direction, with values of up to 0.095 nT/m, and one to the south of East–Southeast Cays Island, represented by a value of 0.062 nT/m. A magnetic low of −0.0360 nT/m is observed over the Nutibara Depression, which coincides with the thickest depositional area in the basin. Moreover, it can be observed how the foci of magnetic anomalies at depth are represented on the surface through bathymetry, evidenced by the geomorphological diversity (Figure 5).

After the residual component separation grid was obtained, vertical derivative filtering was performed. The trends of the magnetic highs were more marked in the northeast direction over the Nutibara Depression area, as well as over the Providencia Depression and the Albuquerque Spur, which are areas with visible faults in bathymetry (Figure 6).

The separation of the regional components was applied to the grid generated from pole reduction by interactive filtering to highlight the magnetic anomalies generated by sources farther away from the surface. This indicates a trend of magnetic highs, with values of 226.21 nT over the Nutibara Depression. The positive anomaly is slightly centralised, but still maintains a northeasterly lineament. However, the magnetic lows were still preserved towards Albuquerque Cays Island (Figure 7).

4.3. Spectral analysis

A spectral analysis was performed on the corresponding map of the residual separation (Figure 7): The first segment (red) corresponds to the contribution of the deep, or

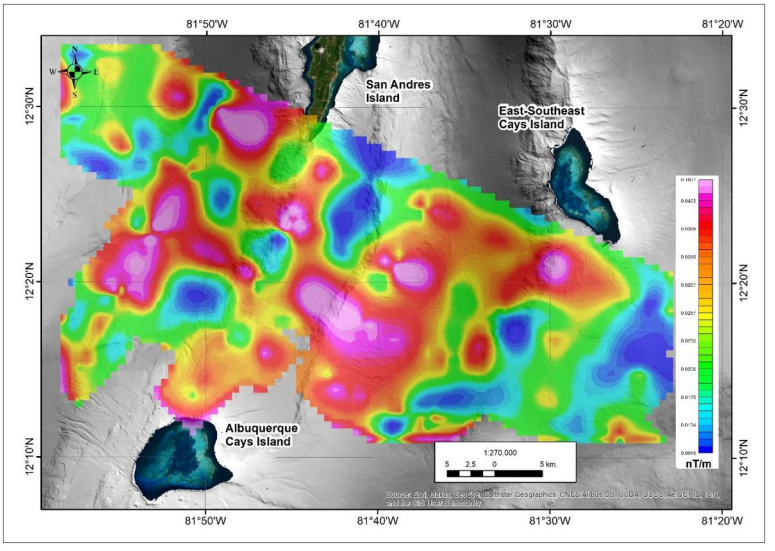

Figure 5. Magnetic map of the analytic signal of the residual field. The map reflects the process of centralization and the definition of residual anomaly edges.

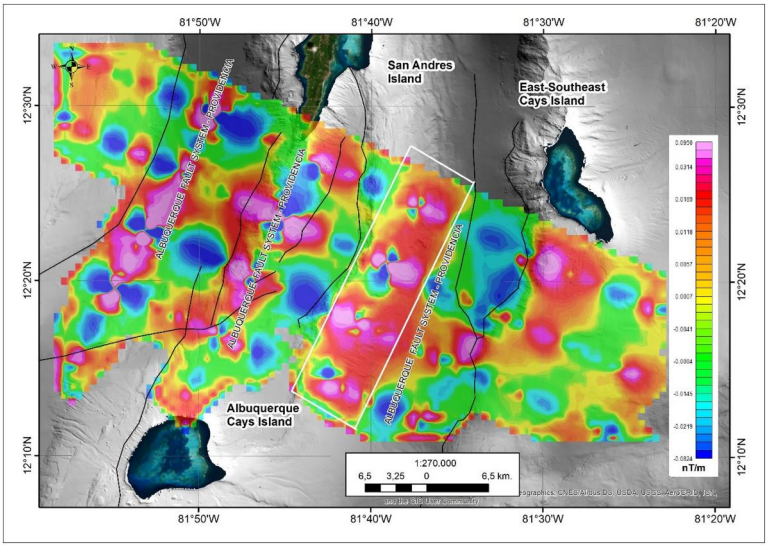

Figure 6. Map showing the vertical (z) derivative of the total magnetic field grid. Grey background is the bathymetry map from the ArcGIS Ocean Base Map. Solid black lines show the surface faults.

regional, source, with frequencies lower than 0.12 km^{-1}, and which therefore generates wavelength anomalies greater than 4 km up to 5 km. The second segment (blue) corresponds to the intermediate source, with frequency values between 0.12 km^{-1} and 0.26 km^{-1}, corresponding to wavelength anomalies between 4 km and 2.5 km, respectively. The third segment (green) is associated with the shallowest sources, for frequencies between 0.26 km^{-1} and greater than 0.56 km^{-1}, generating wavelength anomalies between 2.5 km and wavelengths less than 0.5 km (Figure 8).

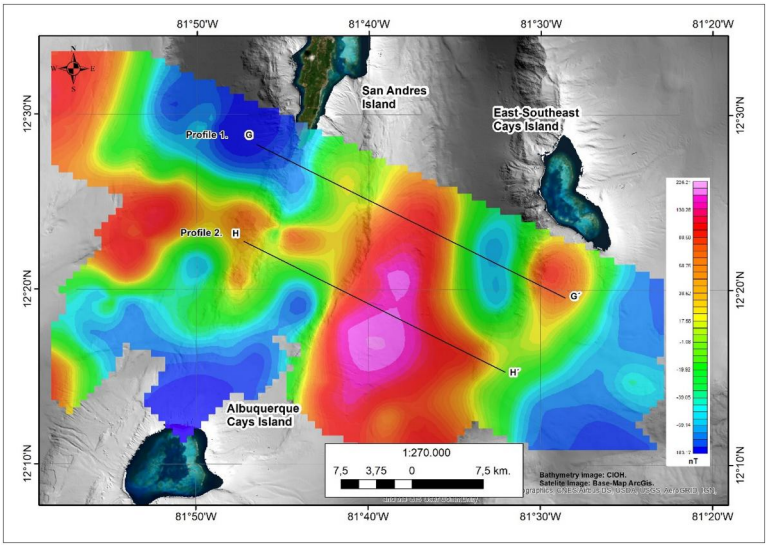

Figure 7. Map showing the regional separation of the deepest sources. Profile 1 and Profile 2 are intended to compare the behaviour of the submarine relief with the regional field displayed.

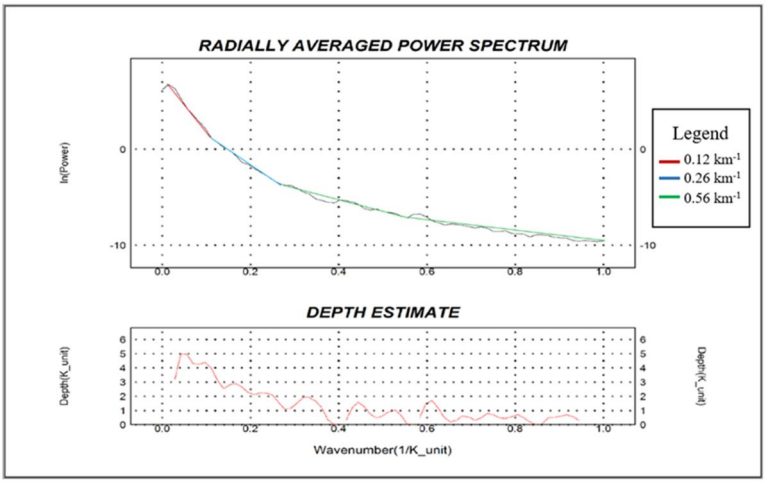

Figure 8. Display of the cut-off wavelength ($K = 0.14$). Window showing the change in slope. It is interpreted as segments with wavelength ranges representing the depth of the sources. Top: Shows the power intensity by generating a radially averaged power spectrum from an image obtained by Fast Fourier Transform (residual separation surface). Bottom: Estimation of the source depth in km based on the radially averaged power spectrum of the anomalies.

4.4. Euler deconvolution (DoE)

Part of the data surface obtained through the DoE showed elongated anomalies linked to the northeastward lineaments (Figure 7) and shapes associated with magnetised elongated bodies. Assuming these are possible magnetic bodies, a structural index of '1.0' is specified. The estimated surface was presented as a colour palette (Figure 9).

The obtained map (Figure 10) shows the solutions represented on the DoE surface. The analytic signal is plotted in greyscale with symbols to present the following results: in blue, the shallowest anomaly sources are located at depths up to 1000 m; in green, the

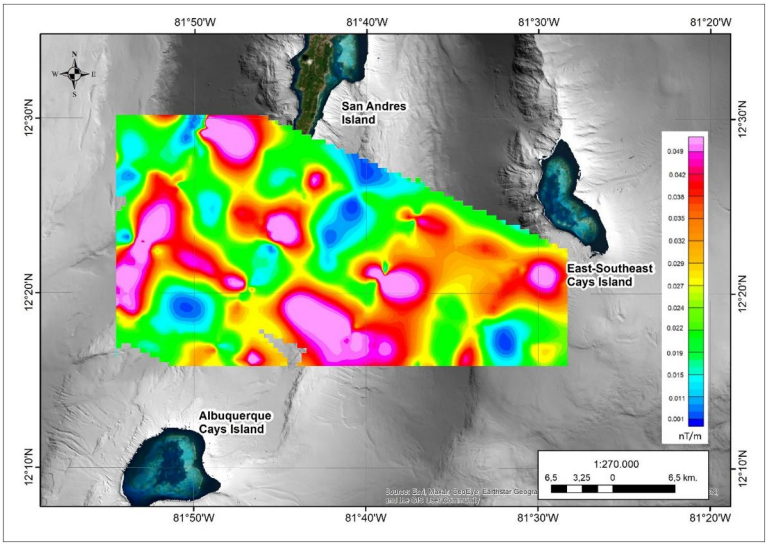

Figure 9. Signal map visualization by using Euler deconvolution. Grey background is the bathymetry map from the ArcGIS Ocean Base Map.

sources are located at depths ranging from 1000 to 2000 m; in yellow, the bodies are slightly deeper, between 2000 and 3000 m deep; and finally, in the larger red symbols, the sources are at depths greater than 3000 m.

4.5. Profiles

To establish the relationship between bathymetry and magnetism, two profiles were made perpendicular to the seafloor features (Figure 7), which have linear northeast-trending characteristics.

When performing profile 1 (Figure 11) on the two surfaces, a relationship between the relief shape and the residual magnetic anomaly curve was observed, where the boundary between the Nutibara Depression and Wayuu Spur had the most representative magnetic high in the study area (106.3 nT). There is also a relationship between the two magnetic lows that are located on the two depressions (San Andres with −145.6 nT and Nutibara with −62.2 nT).

In profile 2 (Figure 11), a relationship between bathymetry and the curve described by the magnetic signal was observed. The magnetic lows are strongly pronounced over the depressions of San Andres and Albuquerque Cays Island with values of −62.03 nT and −77.30 nT, respectively. In the Wayuu Spur area, the most pronounced magnetic high is preserved at 171.65 nT.

5. Discussion

5.1. Low resolution and free data NOAA

In the methodological paper of the work presented in this article (Oviedo et al. 2020), our data were compared with sounding data obtained from the National Oceanic and Atmospheric Administration (NOAA) magnetic data repository in the same study area. Despite the long interval between the two surveys, almost 50 years, no significant

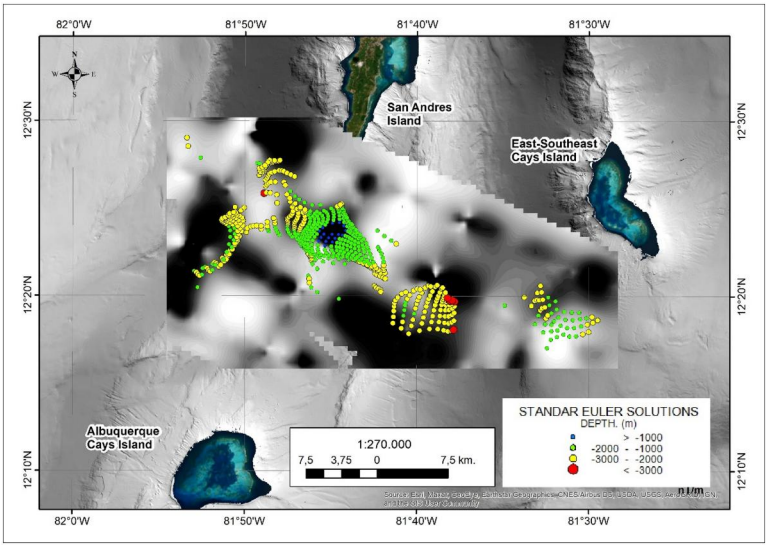

Figure 10. Visualization of the depth estimation of anomaly-generating sources, performed by the Euler deconvolution (DoE) method.

differences were observed for the magnetic variables analysed. Finally, the results show small differences between the magnetic data obtained for the years 1970 and 2018.

The magnetic information downloaded from NOAA (2021) has an extension MGD77T and contains the positions of the tracking line and data with corrections for diurnal variation and IGRF. However, no pole-reduction filters or positioning corrections were indicated within the NOAA metadata. For viewing on a common surface, the two geodatabases were joined and charted to WGS 1984 UTM Zone 17 N, corresponding to the projection of the study area. With the positional and magnetic intensity data, a magnetic surface was generated (Figure 12), as presented in the methodological article, where the positive anomalies were similarly identified on the Wayuu Spur and the Nutibara Depression to the east and northwest, respectively, at the low Nicaraguan elevation. Regarding negative anomalies, the magnetic basement located in the areas near Albuquerque Cays Island stands out (Oviedo et al. 2020).

5.2. Low-resolution and free data GeoMapApp

Additional analyses were performed at the same location as profile 1 (G-G' in Figure 11), with free data available in the GeoMapApp service (version 3.7.1; Figure 13), where they were superimposed on the same profile of the Global Multi-Resolution Topography (GMRT) data grid, which compiles edited multibeam sonar data provided by institutions worldwide and merged into an updated grid of global elevation data. The magnetic grid was constructed using the EMAG2 model Version 3, based on terrestrial magnetic anomalies with a resolution of 2 arc min, and compiled from satellite, naval, and airborne magnetic measurements.

Related to the relationship commented previously between bathymetry and the curve described by the magnetic signal, evidence allows us to conclude that at least the atolls, islands, and coral banks in the south of the archipelago may have originated as volcanoes or geoforms with high ferrous content (Geister and Diaz 2007). About the magnetic observed in the depressions of San Andres and Albuquerque Cays Island, subsidence and

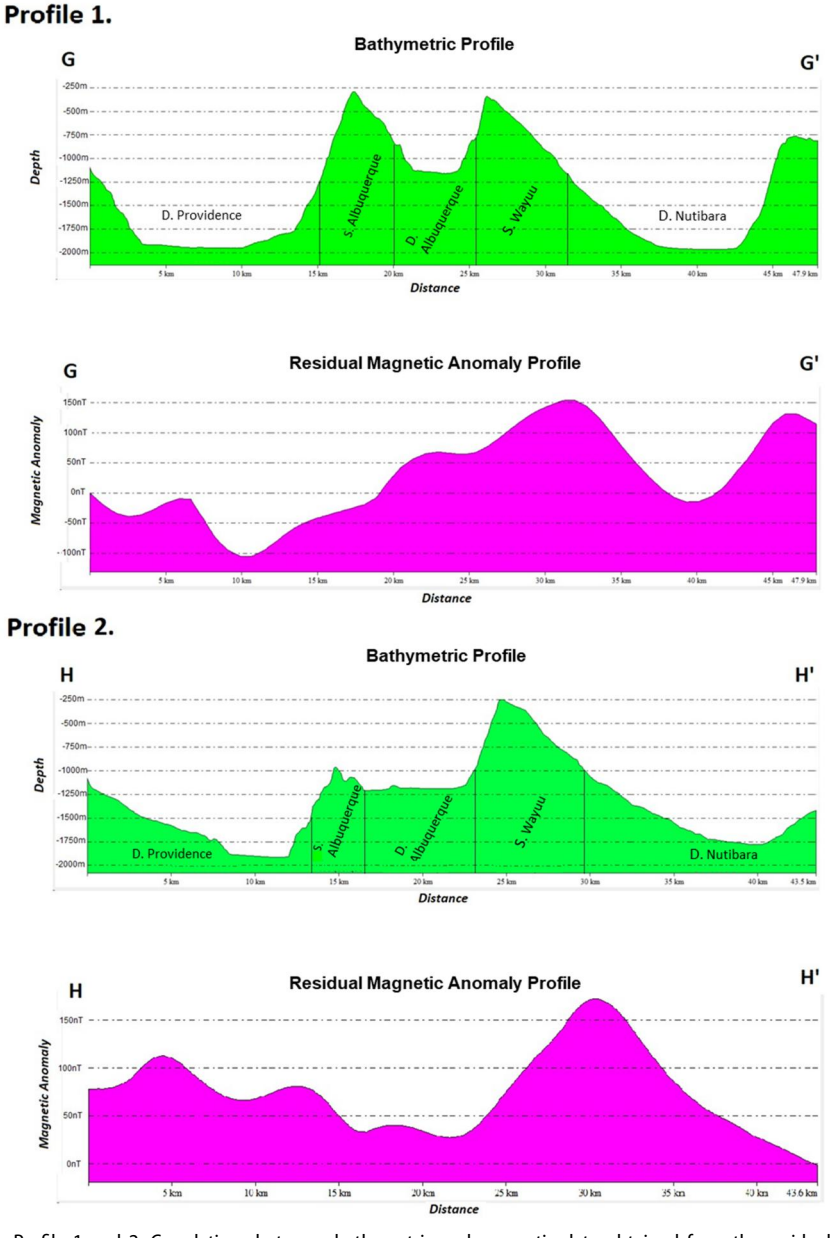

Figure 11. Profile 1 and 2. Correlations between bathymetric and magnetic data obtained from the residual field surface and bathymetry.

simultaneous coverage with carbonates in the shallow zones of the volcanic summits from the Cenozoic to the Quaternary allowed the formation of shallow banks and atolls in the archipelago, which may be the reason for this low magnetic response. Finally, superimposing the magnetic information of the area with high-resolution gravity surfaces would help in the future to understand in a more approximate way the conformation of these insular bodies (Diaz et al. 1996).

Moreover, information about the correlations between bathymetric and magnetic data (Figure 11) also allowed us to establish magnetic anomaly relationships generated by the

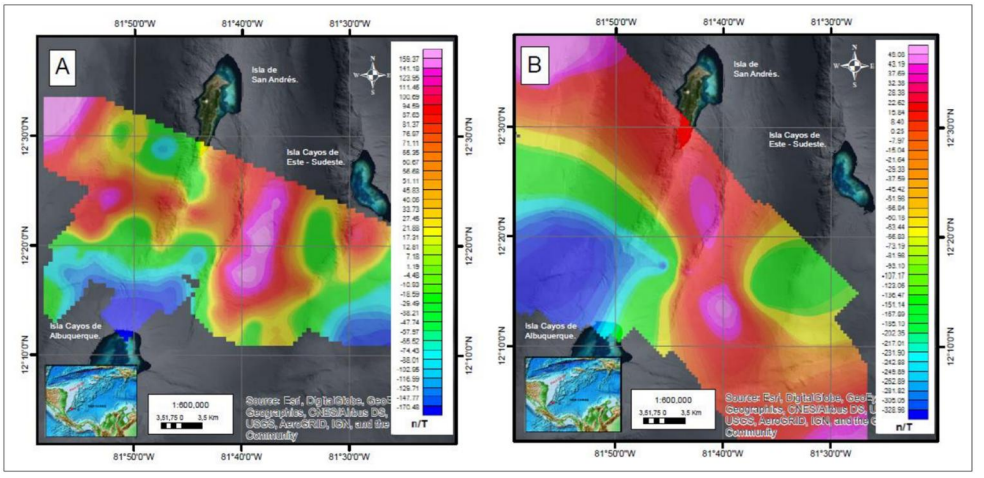

Figure 12. Survey application in the Colombian Caribbean 2018 (a), contrasted with data collected by NOAA in 1970 (B). Adapted from Oviedo et al. (2020).

geoforms present in the study area. Regional information, which is freely accessible and has been presented with lower resolution, allows for the observation of a positive anomaly to the east, which coincides with a positive peak in the magnetic anomaly at the location of the Nutibara Depression (Figure 12). Comparing both figures (Figure 12(A,B)), we can establish that a positive magnetic anomaly is still present, even in the EMAG2 model, but it is not possible to associate it directly with a geomorphological reference present on the seafloor.

5.3. Comparison with other researchers

The magnetic highs obtained in the data grids over East-Southeast Cays Island and in the vicinity are from formations rising from the seafloor to depths of more than 1000 m. These may be associated with the formation of igneous origins or basalts that could be lodged near the seafloor surface, generating positive variations in the magnetic readings (Figure 4). Apparently, they have a volcanic basement, indicating that the magnetic anomalies detected in the surroundings of San Andres Island and East-Southeast Cays Island are due to atolls and volcanic islands, which is consistent with the results of previous studies (Mauffret and Leroy 1997; Osorio-Granada et al. 2022). Evidence of this is a dredged volcanic sample from Albuquerque Cays Island (Diaz et al. 1996), and volcanic rocks from Providence Island (Geister 1992). This information provides a geological basis for the results obtained in this study, where the deepest sources have the most representative magnetic highs and appear to be located at a depth of approximately 5 km, according to the spectral analysis of the acquired data. Additionally, Carvajal Arenas (2017) presents gravity-magnetic correlation models with seismic profiles, which indicate that the high amplitude of the magnetic anomaly supports magnetisation similar to a volcanic origin (Milliman 1969).

Moreover, magnetic lows were observed over Albuquerque Cays Island, which may be associated with the subsidence and simultaneous coverage of these volcanoes by shallow-water carbonate layers from the Cenozoic to the Quaternary, leading to the formation of shallow banks and atolls of the archipelago (Milliman 1969; Geister and Diaz 2007). In addition, according to Pindell et al. (2006), Milliman and Supko (1968) obtained the first

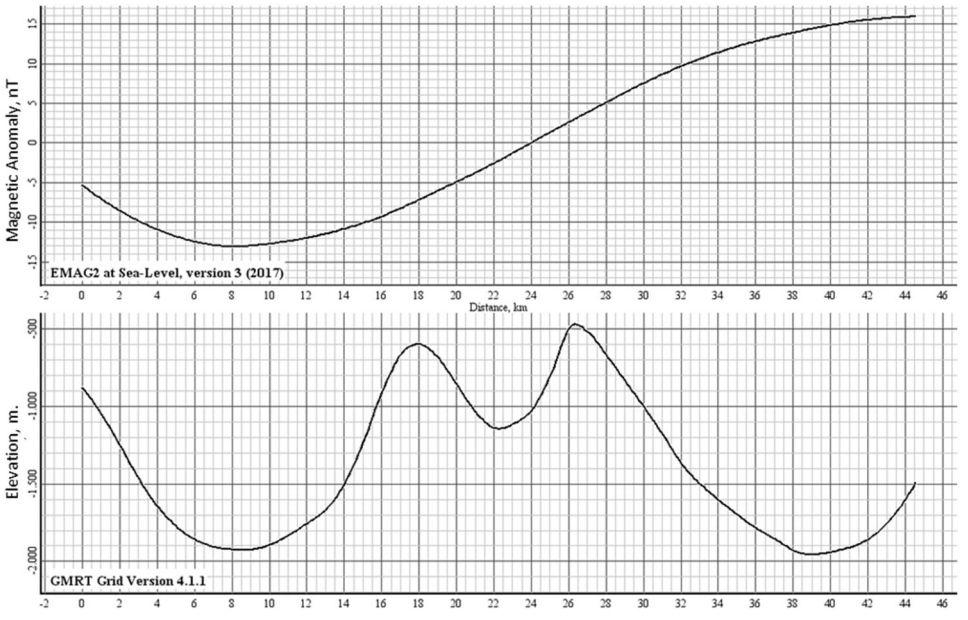

Figure 13. Bathymetric and magnetometry comparison profile 3. Correlation profiles between bathymetry and magnetic data obtained from the free data in GeoMapApp.

geomagnetic profiles during a cruise to the San Andres area. By superimposing this information on the submarine topography, a relationship that is particularly pronounced in East-Southeast Cays Island is revealed. This indicates possible deep volcanic cones under the limestone cover of the atolls and San Andres Island. The volcanic origin of the cones is further supported by a basaltic fragment dredged at a depth of 700 m near Albuquerque Cays Island during the same campaign.

Leroy et al. (2000) conducted correlation studies of magnetic and bathymetric data in the Caribbean, more explicitly in the Cayman Trench, where they were able to interpret that the history of the Cayman Trench is directly related to global plate kinematics with convergence events. These conclusions were drawn from the interpretation of superimposed synthetic magnetic models and correlated with the bottom topography, indicating that this is a zone of oceanic divergence that began at the beginning of the Eocene.

In this analysis, it can be corroborated, as in our study area, that the magnetic peaks, whether positive or negative, coincide with the high and low peaks present in the submarine relief, establishing that there is a relationship between the two sources of information. This also coincides with the principle of the geophysical method, which states that it can be used to identify areas of oceanic divergence and areas of energy release, such as volcanoes.

6. Conclusions

The present study allows the identification of the relief and geomagnetic characterisation of the subsoil of the area, demonstrating that the techniques and methods developed by the authors and the Colombian maritime general direction provide valuable information for the analysis and characterisation of marine geomorphology, which in turn becomes scientific support for the defense of the Colombian sovereignty of its maritime territory.

Advanced magnetometry technology, combined with high-resolution bathymetry, allows us to characterise the behaviour of the submarine relief and establish the possible geological and geophysical processes that have given rise to its modelling. Similarly, the magnetic information in this study identified suspected sources of magnetic anomalies that could be associated with volcanic processes that are not yet evident on the surface of the seabed.

The bottom geomorphology is strongly related to the signatures described by the residual magnetic anomalies, which indicate the presence of magnetic highs that may be associated with basement highs and volcanic cones with elongated shapes in the northeast direction due to ocean floor faults. On the other hand, the most representative magnetic lows of the study area were located over the area of Albuquerque Cays Island. This may be due to the masking of the magnetic signal by the presence of coral structures characterised by low magnetic responses.

The results of the spectral analysis show that the shallowest sources are in the first 500 m depth with frequencies of 0.26 km^{-1} and above 0.56 km^{-1}, while the deepest sources are located between 4 and 5 km depth with representative frequencies below 0.12 km^{-1}. The results are in contrast with the results obtained with the DoE method and show that the anomaly-generating bodies are mostly located between 1000 and 3000 m depth, reaching depths greater than 3000 m, which can be correlated with the spectral analysis, enabling the validation of data processing.

Disclosure statement

No potential conflict of interest was reported by the author(s).

Acknowledgments

This work was possible thanks to the support of the 'Marine Geomagnetism' project, founded by the General Maritime Directorate (DIMAR). We also thank the Directorate of DIMAR and CIOH for their support in fieldwork and authorisation for the use of data in the preparation of this document. The authors thank the crew of the ARC Roncador Oceanographic Research Vessel and the staff of the CIOH Hydrographic Survey for their collaboration during the survey campaigns and data processing.

Funding

APC was funded by the University of Cádiz and RNM912 Coastal Engineering Research Group. The UCA research stay in Cartagena de Indias (Colombia) was funded by the University of Cadiz, and supported in Colombia by ENAP (Escuela Naval de Cadetes 'Almirante Padilla'). The authors thank the two anonymous reviewers and the editor for their comments and suggestions, which have allowed us to significantly improve the ms.

References

[CIOH] Centro de Investigaciones Oceanográficas e Hoidrográficas. 2024. Secciones/Sección Servicio de Hidrografía/Productos y Servicios/Levantamientos/Levantamientos Hidrograficos. Accessed on: https://cioh.dimar.mil.co/index.php/es/areas-del-conocimiento/hidrografia/arhid-productos-y-servicios/levantamientos-hidrografia/levantamientos-hidrograficos-arhid.

[IHO] International Hydrographic Organization. 2020. International hydrographic organization standards for hydrographic surveys S-44 Edition 6.1.0. Monaco: International Hydrographic Organization. Available from: https://acortar.link/UQUlQP.

[UN] United Nations. 1982. Convención de las Naciones Unidas sobre el Derecho del Mar. https://www.un.org/depts/los/convention_agreements/texts/unclos/convemar_es.pdf.

Alatorre-Zamora MA, Rosas-Elguera J, Pérez-Rodríguez G, Campos-Enríquez JO, Maciel-Flores R. 2012. 3D Euler deconvolution and analytic signal contributing to fault risk analysis in The Valle de Banderas. Graben. 10(1):1–31. www.e-gnosis.udg.mx/vol10/art1.

Alken P, Thebault E, Beggan CD, Amit H, Aubert J, Baerenzung J, Bondar TN, Brown WJ, Califf S, Chambodut A, et al. 2021. International geomagnetic reference field: the thirteenth generation. Earth Planets Space. 73(1):1–25. doi:10.1186/S40623-020-01288-X/FIGURES/5.

Bajgain SK. 2011. Gravity and magnetic modeling of basement beneath Alabama Gulf Coastal Plain [Degree Master Science Thesis]. Montgomery (AL): Auburn University, Department of Geology and Geography. https://acortar.link/H9wqBa.

Bernabéu A, Medina R, Vidal C, Muñoz Pérez JJ. 2001. Estudio morfológico del perfil de playa: modelo de perfil de equilibrio en dos tramos. Rev Soc Geol de España. 14(3–4):227–236. Available from: https://rodin.uca.es/handle/10498/15916.

Berrocoso Domínguez M, Jigena B, Mamani R, Muñoz-Pérez JJ, Walliser J, Calderay F. 2018. Metodología para la gestión de la información hidrológica en vías fluviales: aplicación a Bolivia. Available from: https://rodin.uca.es/xmlui/handle/10498/20851.

Berrocoso M, Fernández-Ros A, Ramírez ME, Salamanca JM, Torrecillas C, Pérez-Peña A, Páez R, García-García A, Jiménez-Teja Y, García-García F, et al. 2008. Geodetic research on deception island and its environment (South Shetland Islands, Bransfield Sea and Antarctic Peninsula) During Spanish Antarctic Campaigns (1987–2007). Geodetic Geophys Observ Antarctica. 97–124. doi:10.1007/978-3-540-74882-3_6.

Blakely RJ, Wells RE, Weaver CS, Johnson SY. 2002. Location, structure, and seismicity of the Seattle fault zone, Washington: evidence from aeromagnetic anomalies, geologic mapping, and seismic-reflection data. Geological Society of America Bulletin. 114(2):169–177. doi:10.1130/0016-7606(2002)114<0169:LSASOT>2.0.CO;2.

Carvajal Arenas LC. 2017. Hydrocarbon prospectivity of the Nicaraguan Rise and Colombia Basin, western Caribbean Sea [PhD thesis]. University of Houston.

Case JE, MacDonald WD, Fox PJ. 1990. Caribbean crustal provinces; seismic and gravity evidence. Caribbean Region. Vol H: 15–36.

Catalán M, Martos YM. 2022. New evidence supporting the Pacific Mantle Outflow: hints from crustal magnetization of the Phoenix Plate. Remote Sensing. 14(7):1642. doi:10.3390/rs14071642.

Diaz JM, Sanchez JA, Zea S, Garzon-Ferreira J. 1996. Morphology and marine habitats of two Southwestern Caribbean Atolls: Albuquerque and Courtown. Atoll Research Bulletin No. 435. Available from: https://acortar.link/Dq1JeJ.

DIMAR, Pelaez J, Oviedo K. 2015. Manual de adquisición y procesamiento de información geomagnética. Colombia: DIMAR. p. 180.

Driscoll NW, Diebold JB. 1998. Deformation of the Caribbean region: one plate or two? GeoScienceWorld. 26(11):1043. https://pubs.geoscienceworld.org/gsa/geology/article-abstract/26/11/1043/206786/Deformation-of-the-Caribbean-region-One-plate-or?redirectedFrom=fulltext. doi:10.1130/0091-7613(1998)026<1043:DOTCRO>2.3.CO;2.

Eppelbaum L. 2019. Geophysical potential fields: geological and environmental applications. In: Computational geophysics series. Vol. 2. Amsterdam: Elsevier. ISBN: 978-0-12-819646-5. Available from: https://acortar.link/5qcm1h.

Finn C, Williams DL. 1987. An aeromagnetic study of Mount St. Helens. J Geophys Res. 92(B10):10194–10206. doi:10.1029/JB092iB10p10194.

Flanagan G, Williams DL. 1982. A magnetic investigation of Mount Hood, Oregon. J Geophys Res. 87(B4):2804–2814. doi:10.1029/JB087iB04p02804.

Galvan PJ. 2016. Metodos potenciales y electromagneticos aplicados a la modelacion bidimensional del volcan tipo maar ¨La Joyuelä [Tesis de Máster]. San Luis Potosi, Mexico: Instituto Potosino de Investigacion Cientifica y Tecnologica, A.C., Laboratorio de Geofísica. https://acortar.link/gh3Q0C.

Geister J. 1992. ERLANGEN 1992 Modern Reef Development and Cenozoic Evolution of an Oceanic Island/Reef Complex : Isla de Providencia (Western Caribbean Sea, Colombia). Facies. 27(1):1–69. doi:10.1007/BF02536804.

Geister J, Diaz J. 2007. Ambientes arrecifales y geología de un archipiélago oceánico: San Andrés, Providencia y Santa Catalina. Mar Caribe, Colombia (con Guía Campo). Bogotá: Instituto Colombiano de Geología y Minería (INGEOMINAS). Available from: https://acortar.link/k9SEdA.

Geometrics Inc. 2018. MagLogPro™ & MagLogLite™. Data acquisition software, 25479-01 Rev. R, User's Guide. Available from: https://www.geometrics.com/wp-content/uploads/2018/10/MagLogManual.pdf.

Geometrics Inc. 2020. G-882 Cesium Marine magnetometer operation manual [accessed 2023 March 23]. Available from: https://acortar.link/uEwv1O

Grandis H, Dahrin D. 2017. The utility of free software for gravity and magnetic advanced data processing. IOP Conf Ser Earth Environ Sci. 62(1):012046. doi:10.1088/1755-1315/62/1/012046.
Granot R, Dyment J. 2019. The influence of post-accretion sedimentation on marine magnetic anomalies. Geophys Res Lett. 46(9):4645–4652. doi:10.1029/2019GL082265.
Hanna WF. 1990. Geologic applications of modern aeromagnetic surveys. William F. Hanna, editor. Colorado: U.S. Geological Survey Bulletin 1924. p. 116. Available from: https://pubs.usgs.gov/bul/1924/report.pdf.
Holcombe TL, Ladd JW, Westbrook GK, Edgar NT. 1990. Caribbean marine geology; ridges and basins of the plate interior. The Caribbean Region, The Geology of North America, Vol. H. Colorado: Geological Society of America. p. 231–260.
Honkura Y, Okubo Y, Nagaya K, Makino M, Oshima S. 1991. A magnetic anomaly map in the japanese region with special reference to tectonic implications. J Geomagn Geoelec. 43(1):71–76. doi:10.5636/jgg.43.71.
Idárraga-García J, León H. 2019. Unraveling the underwater morphological features of Roncador Bank, Archipelago of San Andres, Providencia and Santa Catalina (Colombian Caribbean). Front Mar Sci. 6(FEB):77. doi:10.3389/fmars.2019.00077.
Jacobs JA. 1994. Reversals of the Earth's magnetic field. 2nd ed. Vol. 63. Cambridge: Cambridge University Press; p. 346. Available from: https://acortar.link/gTUDFN.
Jigena-Antelo B, Estrada-Ludeña C, Howden S, Rey W, Paz-Acosta J, Lopez-García P, Salazar-Rodriguez E, Endrina N, Muñoz-Pérez JJ. 2023. Evidence of sea level rise at the Peruvian coast (1942–2019). Sci Total Environ. 859(Pt 2):160082. doi:10.1016/j.scitotenv.2022.160082.
Jigena B, Berrocoso M, Torrecillas C, Vidal J, Barbero I, Fernandez-Ros A. 2016. Determination of an experimental geoid at Deception Island, South Shetland Islands, Antarctica. Antarct Sci. 28(4):277–292. doi:10.1017/S0954102015000681.
Jigena B, Vidal J, Berrocoso M. 2015. Determination of the mean sea level at deception and Livingston Islands. Antartic Science. 27(1):101–102. doi:10.1017/S0954102014000595.
Kongsberg. 2023. Versions of EM 302. EM Series Multibeam echo sounders. Instruction Manual. [accesed 2023 April 18]. Available from: https://acortar.link/BrdxvP
Leroy S, Mauffret A, Patriat P, Mercier de Lepinay B. 2000. An alternative interpretation of the Cayman trough evolution from a reidentification of magnetic anomalies. Geophys J Int. 141(3):539–557. https://academic.oup.com/gji/article/141/3/539/612159. doi:10.1046/j.1365-246x.2000.00059.x.
López-Loera H, Tristán-González M, Luis Potosí S, Potosí L. 2013. Geology and magnetometry of the Villa de Reyes graben, San Luis Potosí, Mesa Central, Mexico: Tectonic implications. Boletín de la Sociedad Geologica Mexicana. 65(1):137–156.
MacLeod IN, Jones K, Dai TF. 1993. 3-D analytic signal in the interpretation of total magnetic field data at low magnetic latitudes. Explor Geophys. 24(3–4):679–687. doi:10.1071/EG993679.
Mauffret A, Leroy S. 1997. Seismic stratigraphy and structure of the Caribbean igneous province. Tectonophysics. 283(1–4):61–104. doi:10.1016/S0040-1951(97)00103-0.
Milliman JD, Supko PR. 1968. On the geology of San Andres Island, western Caribbean. Geol Mijnbouw. 47:102–105.
Milliman JD. 1969. Four Southwestern Caribbean Atolls: Courtown Cays, Albuquerque Cays, Roncador Bank and Serrana Bank. Atoll Res Bull. 129:1–26.
Narvaez Medina L. 2012. Modelo de fuentes de anomalías Geomagneticas de Campo Total asociadas al estado de la cámara magmática del volcán Galeras. Universidad Nacional de Colombia. p. 115. http://www.bdigital.unal.edu.co/39635/.
Nwankwo UC, Howden S, Wells D, Connon B. 2020. Validation of VDatum in Southeastern Louisiana and Western Coastal Mississippi. Mar Geod. 44(1):1–25. doi:10.1080/01490419.2020.1846644.
Osorio-Granada AM, Jigena-Antelo B, Vidal Pérez JM, Hernández-Pardo O, León-Rincón H, Muñoz-Pérez JJ. 2022. Potential fields modeling for the Cayos Basin (Western Caribbean Plate): Implications in basin crustal structure. Mar Geol. 449:106819. doi:10.1016/j.margeo.2022.106819.
Oviedo K, Jigena Antelo B, Otálora N, Romero J, Contreras-de-Villar F, Muñoz-Pérez JJ. 2020. A new method for the collection of marine geomagnetic information: survey application in the Colombian Caribbean. JMSE. 9(1):10. doi:10.3390/jmse9010010.
Parker RL, Huestis SP. 1974. The inversion of magnetic anomalies in the presence of topography. J Geophys Res. 79(11):1587–1593. doi:10.1029/JB079i011p01587.
Payo A, Antelo BJ, Hurst M, Palaseanu-Lovejoy M, Williams C, Jenkins G, Lee K, Favis-Mortlock D, Barkwith A, Ellis MA. 2018. Development of an automatic delineation of cliff top and toe on very irregular planform coastlines (CliffMetrics v1.0). Geosci Model Dev. 11(10):4317–4337. doi:10.5194/gmd-11-4317-2018.

Pindell J, Kennan L, Stanek KP, Maresch WV, Draper G. 2006. Foundations of Gulf of Mexico and Caribbean evolution: eight controversies resolved. Geol Acta Int Earth Sci J. 4:1–2.

Quintero W, Ladino A, Lozano E, Bolívar O, Rincón J, Puentes M. 2014. Mapa de profundidad de la isoterma de Curie para Colombia Versión 0. Bogota: Servicio Geologico Colombiano.

Rey W, Ruiz-Salcines P, Salles P, Urbano-Latorre CP, Escobar-Olaya G, Osorio AF, Ramírez JP, Cabarcas-Mier A, Jigena-Antelo B, Appendini CM. 2021. Hurricane flood hazard assessment for the Archipelago of San Andres, Providencia and Santa Catalina, Colombia. Front Mar Sci. 8:1612. doi:10.3389/FMARS.2021.766258/BIBTEX.

Seequent. 2022. Better in ten – Oasis montaj, Oasis montaj How-to Guide. Available from: https://www.seequent.com/help-support/oasis-montaj/.

Teledyne. 2021. Inicio | Teledyne CARIS. https://www.teledynecaris.com/en/home/.

Telford WM, Gerald LP, Sheriff RE. 1990. Applied geophysics. 2nd ed. Cambridge, UK: Cambridge University Press; p. 760. Available from: https://acortar.link/uv3jo1.

Whitehead N, Musselman C. 2007. Montaj MAGMAP Filtering. 69. www.geosoft.com.

Zou Z, Bakhtiari Rad P, MacElloni L, Zhang L. 2021. Temporal and spatial variations in three-dimensional seismic oceanography. Ocean Sci. 17(4):1053–1066. doi:10.5194/os-17-1053-2021.